Volumetric Evaluation of 3D Multi-Gradient-Echo MRI Data to Assess Whole Liver Iron Distribution by Segmental R_2^* Analysis: First Experience

Volumetrische Auswertung von 3D-Multigradientenecho-MRT-Daten zur Beurteilung der Eisenverteilung in der gesamten Leber durch segmentale R_2^*-Analyse: erste Erfahrungen

Authors

Arthur P Wunderlich[1, 2], Holger Cario[3], Stephan Kannengießer[4], Veronika Grunau[1], Lena Hering[1], Michael Götz[2], Meinrad Beer[1], Stefan Andreas Schmidt[1]

Affiliations

1 Diagnostic and Interventional Radiology, University Ulm Medical Centre, Ulm, Germany
2 Section for Experimental Radiology, University Ulm Medical Centre, Ulm, Germany
3 Department of Pediatrics and Adolescent Medicine, University Ulm Medical Centre, Ulm, Germany
4 Magnetic Resonance Development, Siemens Healthcare AG, Erlangen, Germany

Key words

MR-imaging, liver, iron overload, thalassemia

received 13.07.2022
accepted 21.10.2022
published online 2023

Bibliography

Fortschr Röntgenstr 2023; 195: 224–233
DOI 10.1055/a-1976-910
ISSN 1438-9029

Georg Thieme Verlag KG, Rüdigerstraße 14,
70469 Stuttgart, Germany

Correspondence

Dr. Arthur P Wunderlich
Klinik für Diagnostische und Interventionelle Radiologie,
Universitätsklinikum Ulm, Albert-Einstein-Allee 23,
89070 Ulm, Germany
Tel.: +49/7 31/50 06 10 86
Fax: +49/7 31/50 06 11 08
arthur.wunderlich@uni-ulm.de

ZUSAMMENFASSUNG

Ziel Die transversale MR-Relaxationsrate R_2^* hat sich als nützlich für die Überwachung der Eisenüberladung der Leber erwiesen. Mittlerweile steht eine Sequenz zur Verfügung, die die Erfassung der gesamten Leber in einem einzigen Atemzug ermöglicht. Das erlaubt volumetrische Studien der hepatischen R_2^*-Verteilung. Unser Ziel war es, die Machbarkeit einer computergestützten Segmentierung der gesamten Leber aus 3D-Multigradientenecho-MRT-Daten zu untersuchen. Darüber hinaus haben wir untersucht, ob die Bestimmung des R_2^*-Wertes der gesamten Leber mit der Analyse einer einzelnen Schicht vergleichbar ist. Schließlich wurden die segmentalen R_2^*-Unterschiede bewertet.

Methoden 44 Patienten wurden mittels Multi-Gradientenecho-MRT bei 1,5 T untersucht. Die Leber wurde segmentiert und in neun Segmente unterteilt. Die segmentalen R_2^*-Werte wurden für alle Patienten zusammen und unterteilt nach zwei Kriterien analysiert: durchschnittliche R_2^*-Werte und vorherrschender Grund für die Eisenüberladung. Die Korrelation von Einzelschicht- und volumetrischen Daten wurde mit dem Spearman-Rangtest geprüft, während Segment- und Gruppenunterschiede durch Varianzanalyse bewertet wurden.

Ergebnisse Die R_2^*-Werte der Gesamtleber korrelierten hervorragend mit den Einzelschichtdaten ($p < 0{,}001$). Die niedrigsten R_2^*-Werte traten in Segment 1 (S1) auf, die Unterschiede zwischen S1 und anderen Segmenten waren in fünf Fällen signifikant und in zwei Fällen hochsignifikant. Patienten mit niedrigem R_2^* wiesen keine signifikanten Unterschiede auf, Patienten mit hohem R_2^* zeigten signifikante Unterschiede zwischen S1 und den Segmenten 2, 6 und 7. Krankheitsbedingte Unterschiede zu S1 waren in den Segmenten 3 bis 5 und 7 signifikant.

Schlussfolgerungen Die Ergebnisse dieser Studie deuten auf eine Inhomogenität der hepatischen Eisenverteilung hin. Während der niedrige R_2^*-Wert in S1 durch seine besondere Gefäßversorgung erklärt werden kann, sollte die Ursache für segmentale Unterschiede, möglicherweise bedingt durch spezifische Krankheitsbilder, weiter untersucht werden.

Kernaussagen:

- Die R_2^*-Verteilung in der Leber ist nicht so homogen wie bisher angenommen.
- Dies deutet darauf, dass die Lebersegmente nicht nur eine anatomische, sondern auch eine funktionelle Bedeutung haben.
- Die beste Übereinstimmung des R_2^*-Werts eines einzelnen Segments mit dem der gesamten Leber fanden wir in Segment 8.

ABSTRACT

Purpose MR transverse relaxation rate R_2^* has been shown to be useful for monitoring liver iron overload. A sequence enabling acquisition of the whole liver in a single breath hold is now available, thus allowing volumetric hepatic R_2^* distribution studies. We evaluated the feasibility of computer-assisted whole liver segmentation of 3 D multi-gradient-echo MRI data, and compared whole liver R_2^* determination to analyzing only a single slice. Also, segmental R_2^* differences were studied.

Materials and Methods The liver of 44 patients, investigated by multi-gradient echo MRI at 1.5 T, was segmented and divided into nine segments. Segmental R_2^* values were examined for all patients together and with respect to two criteria: average R_2^* values, and reason for iron overload. Correlation of single-slice and volumetric data was tested with Spearman's rank test, segmental and group differences were evaluated by analysis of variance.

Results Whole-liver R_2^* values correlated excellent to single slice data ($p < 0.001$). The lowest R_2^* occurred in segment 1 (S1), differences of S1 with regard to other segments were significant in five cases and highly significant in two cases. Patients with high average R_2^* showed significant differences between S1 and segments 2, 6, and 7. Disease-related differences with respect to S1 were significant in segments 3 to 5 and 7.

Conclusion Our results suggest inhomogeneous hepatic iron distribution. Low R_2^* in S1 may be explained by its special vascularization.

Key Points

- Hepatic R_2^* distribution is not as homogeneous as previously thought.
- Liver segments might have a functional relevance.
- Segmental and total liver R_2^* values coincide best in segment 8.

Citation Format

- Wunderlich AP, Cario H, Kannengießer S et al. Volumetric Evaluation of 3D Multi-Gradient-Echo MRI Data to Assess Whole Liver Iron Distribution by Segmental R_2^* Analysis: First Experience. Fortschr Röntgenstr 2023; 195: 224–233

1. Introduction

Numerous studies have been performed to study the distribution of hepatic proton density fat fraction (PDFF) in nonalcoholic fatty liver disease (NAFLD) patients and healthy subjects (e. g., [1]). Differences between segments have been reported. For the monitoring of liver iron content (LIC), on the other hand, the usefulness of the transverse relaxation rate R_2^* determined by gradient echo for LIC quantification has been shown, which reflects total body iron [2, 3]. Volumetric multi-gradient-echo sequences are available now that allow the acquisition of the entire liver in a single breath hold [4]. Using the multi-echo technique, acquiring several signals with different echo times after one excitation, transverse relaxation rate R_2^* and PDFF can be determined simultaneously in the entire covered region. The suitability of one of these volumetric sequences for the determination of liver iron content has recently been proven by manually placed regions of interest (ROIs) in appropriate liver cross-sectional images [5]. Meanwhile, software solutions are available for automated or semi-automated segmentation of the liver, e. g. a user-corrected template method as described by Mory et al. [6]. This enables the determination of an average R_2^* value for the entire liver and additionally for individual liver segments [7].

The aim of this study was threefold: First, to evaluate whether semiautomatic liver segmentation is feasible on single-breath-hold MR volumetric images. Second, we aimed to determine R_2^* values segment by segment and to check for deviations between the R_2^* values of the individual segments. Third, segmental R_2^* values were studied also in patient groups, subdivided according to average hepatic R_2^* levels on the one hand and the main reasons for iron overload on the other.

2. Methods

The study was conducted according to the Declaration of Helsinki (last revision 2013, Fortaleza, Brazil). After approval by the University's Ethics Committee, patients examined by MRI in our clinic between May 2017 and April 2018 for noninvasive hepatic iron content quantification were included after written informed consent of patients or, in the case of minors, of the parents. MRI investigation was performed at 1.5 T (MAGNETOM Avanto, Siemens Healthcare, Erlangen, Germany) as published before [5]. Briefly, with a multi-echo 3 D GRE sequence the entire liver was acquired in a single breath hold. Six echoes were acquired at echo times (TE) of 1.2, 2.4, 3.6, 4.8, 6, and 9 ms. The 3 D volume consisted of 56 slices with a field of view (FoV) of $400 \times 300 \times 224\,mm^3$ at a voxel size of $2.5 \times 2.5 \times 4\,mm^3$. The acquisition matrix was $160 \times 84 \times 56$. Immediately after data acquisition, R_2^* and PDFF values were determined voxel by voxel in a multi-step fitting process accounting for fat-water signal dephasing, and were displayed as parameter maps [8].

2.1 Single-slice analysis

A single slice was chosen best suited to place three circular ROIs in the liver parenchyma avoiding vessels. The size and R_2^* mean of the ROIs were documented and the weighted R_2^* mean was determined according to the equation:

$$\overline{R_2^*} = \frac{\sum_{i=1}^{3} n_{pix\,i} * R_2^*{}_i}{\sum_{i=1}^{3} n_{pix\,i}}$$

where $R_2^*{}_i$ is the measured average R_2^* in a given ROI, $n_{pix\,i}$ is its number of pixels, and $\overline{R_2^*}$ is the calculated average R_2^* for the single-slice method.

2.2 Volumetric analysis

Image quality of the volumetric sequence was evaluated using a four-point Likert scale with 1 = excellent image quality, 2 = marginal artifacts not compromising liver diagnosis, 3 = image quality impaired by breathing and/or fat-water mismatch (so-called swaps) and 4 = severe image artifacts. Patients in whom the liver was not completely covered, e. g. due to a different breathing position compared to the survey slices or because the liver was not completely depicted in these, and patients with poor image quality (Likert score 3 or 4) of the volumetric sequence were excluded.

The liver was segmented using Liver Health, an additional software tool of the IntelliSpace Portal (ISP, Philips, Hamburg, Germany), by a medical student under the supervision of an experienced radiologist (more than 15 years of liver MRI experience). From the different contrasts offered by the multi-echo sequence, best suited images were chosen. After an initial automatic segmentation, the liver contour was checked on the axial slices as well as coronal and sagittal reconstructions and corrected if necessary. In cases with moderately to highly elevated R_2^* values, the R_2^* map was used to explicitly identify liver boundaries. The time required for user interaction was documented. After complete segmentation of the liver, it was divided into segments using manually placed anatomical landmarks. We used the division proposed by Couinaud/Bismuth with a total of 9 segments [9]. The landmarks for this subdivision were taken from the reference standard and were in detail: right portal vein bifurcation, Vena (V.) cava inferior, V. hepatica dextra, V. hepatica media, Fissura umbilicalis, bifurcation of left portal vein, left hepatic tip, ligamentum venosum, attachment of the ligamentum venosum at the portal vein, and attachment of the ligamentum venosum at the V. cava. Parts of segmented tissue could be selectively excluded by their R_2^* values, e. g. vessels due to their long T_2^* times, so that only the liver parenchyma relevant for iron overload was included. For this purpose, the software created a T_2^* map and set the threshold values for T_2^* to be considered to 1 and 50 ms. These could then be adjusted manually. After segmentation, the software determined the mean values and standard deviations of the R_2^* values of the whole liver and divided by segments. Also, R_2^* histograms could be created for the whole liver and each segment separately. The R_2^* mean value as well as the volume were documented for the entire liver and for each segment.

2.3 Statistics

Statistical analysis was performed with SPSS (V. 27, 2020, IBM, Armonk, NY). All variables were checked for normal distribution using the Shapiro-Wilk test. The R_2^* values determined by the two methods were checked for agreement using linear correlation. The significance of correlation was evaluated with Spearman's rank test.

Segmental R_2^* values were tested for statistically significant differences as described below. Furthermore, they were normalized with the R_2^* of the total liver according to the equation:

$$rR_{2\,Seg}^{*} = \frac{R_{2\,Seg}^{*}}{R_{2\,Liv}^{*}}$$

where $rR_{2\,Seg}^*$ denotes the relative or normalized segmental R_2^* value, $R_{2\,Seg}^*$ the measured R_2^* mean value of the individual segments and $R_{2\,Liv}^*$ the mean R_2^*value of the whole liver. Both the actual R_2^* and rR_2^* values were checked for differences between liver segments by analysis of variance (ANOVA) with repeated measures. For this purpose, sphericity was analyzed in advance using Mauchly's test. Furthermore, an additional Bonferroni correction was performed because of multiple groups. The effect size was calculated according to Cohen.

In addition, we studied whether nonuniform R_2^* distribution depended on R_2^* levels by dividing our participants into two groups according to their average hepatic R_2^* value, group A with $R_2^* < 140\,s^{-1}$, group B with $R_2^* > 140\,s^{-1}$, a threshold which corresponds to the LIC threshold for therapy indication of 4.5 mg/g and a recently published R_2^* calibration for the sequence used [5, 10]. The significance of differences between the two groups was calculated using the Mann-Whitney-U-Test.

Finally, relative segmental R_2^* values were evaluated to determine if there were any differences due to disease. Of particular interest was the reason for iron overload. We divided diseases of study participants into three groups: solely increased iron absorption, but no transfusion (mainly hemochromatosis, group 1) versus transfusion-dependent anemias without markedly increased iron absorption (group 2) and diseases where iron overload was caused by both increased iron absorption and transfusions (group 3). Significance of differences due to diseases was addressed using a Kruskal-Wallis test. Differences between liver segments within the groups were again tested by ANOVA. Analogous to the entire cohort, Mauchly's test was performed in advance, as well as a Bonferroni correction. Again, effect size was calculated according to Cohen.

In all cases, p-values < 0.05 were assumed significant, $p < 0.01$ highly significant.

3. Results

In the chosen time interval, 58 participants were scanned. In all cases, the liver was imaged completely. 30/58 (52 %) of the studies received a Likert score 1 for excellent image quality, 14/58 (24 %) were scored 2. A total of 14/58 participants (24 %) had to be excluded, 10 were scored 3, and 4 received a score of 4. Thus, 44 participants were evaluated (24 m, 20f, age 23.7 ± 13 years (mean ± SD), age range 4.1 to 60.6 years).

The segmentation procedure was completed successfully in all cases. The total time for segmentation varied between 7 and 14 minutes, on average 9 minutes and 26 seconds. ▶ **Fig. 1** shows examples of liver contours and whole-liver histograms for two participants with different average liver R_2^*. Histograms show a positively skewed R_2^* distribution for both participants. For the participant with a higher R_2^*, distribution was broader compared to the other, indicating a relevant number of voxels with R_2^* above the average value for this participant.

The total liver volume for all patients was 1428 ± 483 ml (mean ± SD), and the range of volumes was 329 to 2788 ml. The mean R_2^* value of all patients was 170.2 ± 112.1 s^{-1} (mean ± SD) determined with the ROI-based method and 163.7 ± 112.2 s^{-1}

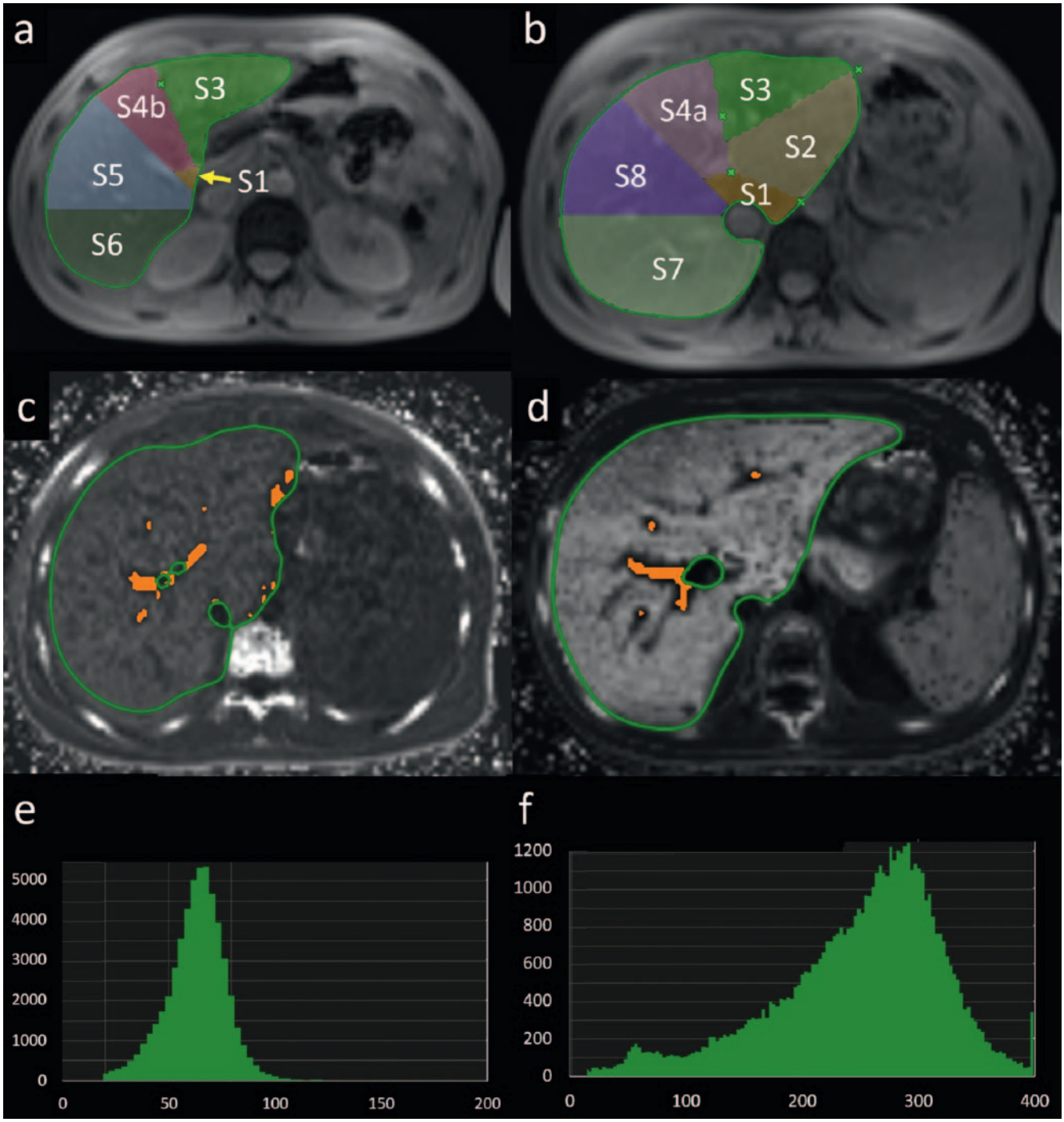

▶ **Fig. 1** Examples of liver segments **(a**, **b)** overlaid on the image with the shortest TE in one representative patient. Subfigures **c** to **f** show two participants, one with low average liver R_2^* **(c**, **e)**, the other with a markedly higher average liver R_2^* **(d**, **f)**. The figure shows the liver contour overlaid on the R_2^* map (panels **c** and **d**, where voxels excluded due to their T_2^* exceeding the given threshold are marked in orange) and whole liver histograms **(e**, **f)**. Note that both histograms are positively skewed, a characteristic which is more pronounced in the participant with a larger average R_2^* **(f)**.

▶ **Abb. 1** Beispiele von Lebersegmenten bei einem repräsentativen Patienten **(a**, **b)**, überlagert auf das Bild mit der kürzesten TE. Die Abbildungen **c** bis **f** zeigen 2 Patienten, einen mit niedrigem durchschnittlichen Leber-R_2^* **(c**, **e)**, den anderen mit deutlich höherem durchschnittlichen Leber-R_2^* **(d**, **f)**. Dargestellt sind die Leberkontur, die der R_2^*-Karte überlagert ist (Teilabb. **c** und **d**, wobei die aufgrund einer Überschreitung des vorgegebenen T_2^*-Schwellenwerts ausgeschlossenen Voxel orange markiert sind), sowie die Histogramme der gesamten Leber **(e**, **f)**. Es fällt auf, dass beide Histogramme eine linksschiefe Verteilung zeigen, eine Eigenschaft, die bei dem Patienten mit dem größeren durchschnittlichen R_2^* stärker ausgeprägt ist **(f)**.

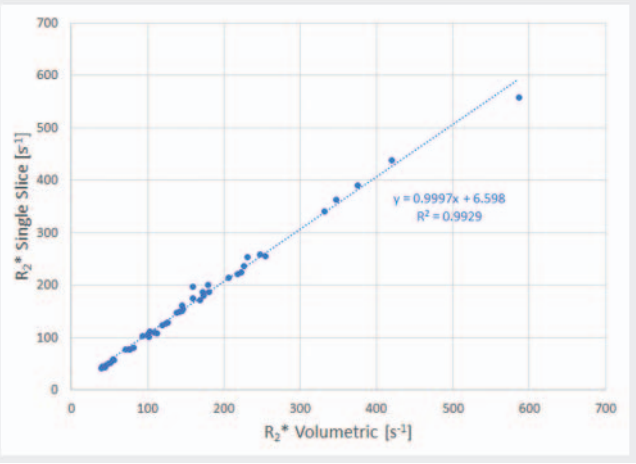

▶ **Fig. 2** Scatterplot of R_2^* values determined with both methods. The dashed line is the regression line. Its equation and coefficient of determination are given. For single-slice analysis, ROIs were placed in the right liver lobe, mostly in segment 8.

▶ **Abb. 2** Streudiagramm der mit beiden Methoden ermittelten R_2^*-Werte. Die gestrichelte Linie ist die Regressionsgerade, ihre Gleichung und ihr Bestimmtheitsmaß sind angegeben. Die ROIs für die Einzelschichtanalyse wurden im rechten Leberlappen platziert, vorwiegend im Segment 8.

(mean ± SD) for the volumetric analysis. The correlation was highly significant with $r = 0.995$, $p < 0.001$. A scatter diagram of the R_2^* values of the different procedures with regression lines is given in ▶ **Fig. 2**. The coefficient of determination $R^2 = 0.993$ indicates a nearly ideal correlation. The regression line was close to identity which indicates congruence of the R_2^* values between the two methods.

The volume averages of the segments are listed in ▶ **Table 1**, as well as the mean actual and normalized R_2^* values. A significantly lower R_2^* in liver segment 1 is noticeable. In contrast, rR_2^* was slightly greater than 1 in other segments, especially in segment 7. In segment 8, the relative R_2^* value was closest to 1, i. e. the actual R_2^* was closest to average hepatic R_2^*.

The relative R_2^* values of the segments are shown in ▶ **Fig. 3**. Significant differences were found for segment 1 compared to the other segments except S4b, with highly significant differences for segments 2 and 7. No significant differences occurred between the other segments 2 to 8.

After dividing patients according to their mean R_2^* value, we got 21 patients (12 m, age 21.8 ± 8.9y [mean ± SD], age range 4.9 to 38.6y) in group A with a mean hepatic $R_2^* < 140\ s^{-1}$ and 23 patients (12 m, age 25.4 ± 15.9 [mean ± SD], age range 4.1 to 60.6y) in group B. Segmental R_2^* distribution was comparable in both groups, as seen from relative R_2^* values shown in ▶ **Table 2**. There were no significant differences in rR_2^* values between the groups for each segment, but significant segmental differences

▶ **Table 1** Various values found for individual segments.

▶ **Tab. 1** Verschiedene Werte der einzelnen Segmente.

	S1	S2	S3	S4a	S4b	S5	S6	S7	S8
Volume [ml]	37.8	191.0	134.5	122.0	83.8	267.6	123.0	210.7	257.7
StdDev Volume	21	88	73	46	36	117	57	87	96
Mean R_2^* [s^{-1}]	151	164	163	164	161	163	165	169	165
SD R_2^*	102	109	109	116	106	111	117	117	116
Significance for R_2^* differences with respect to segment 1 (p)	–	0.0015**	0.039*	0.082	0.2	0.036*	0.031*	0.0006**	0.083
Mean relative R_2^* (rR_2^*)	0.927	1.002	1.006	0.991	0.990	0.987	0.994	1.035	0.999
StdDev relative R_2^*	0.084	0.072	0.081	0.048	0.083	0.057	0.072	0.085	0.049
Significance for rR_2^* differences with respect to segment 1 (p)	–	0.001**	0.004*	0.006*	0.056	0.023*	0.026*	0.0003**	0.001*

Values of the individual segments, averaged over all patients. Significant differences for R_2^* and relative R_2^* values with respect to segment 1 are marked with an asterisk (*), highly significant differences with two asterisks (**).
Werte der einzelnen Segmente, gemittelt über alle Patienten. Signifikante Differenzen der R_2^*- und relativen R_2^*-Werte gegenüber Segment 1 sind mit einem Stern (*) markiert, hochsignifikante Differenzen mit 2 Sternen (**).

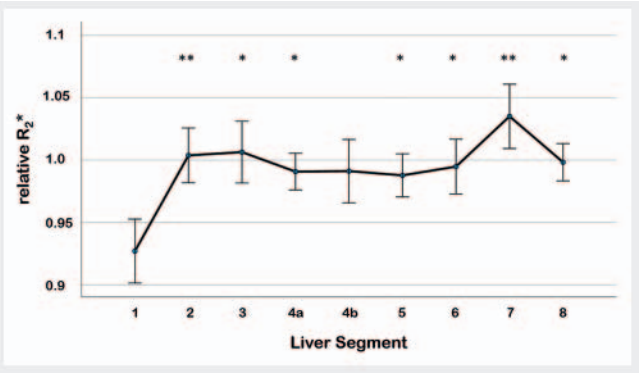

▶ **Fig. 3** Mean values (dots) and 95 % confidence interval (whiskers) for relative segmental R_2^* values. Significant differences with respect to segment 1 are marked by asterisks (* = significant – $p < 0.05$, ** = highly significant – $p < 0.01$). No significant differences of rR_2^* values between other liver segments were found.

▶ **Abb. 3** Mittelwert (Punkte) und 95 % Konfidenzintervall (Balken) für die relativen R_2^*-Werte der Segmente. Signifikante Unterschiede zu Segment 1 sind durch Sternchen gekennzeichnet (* = signifikant – $p < 0{,}05$, ** = hoch signifikant – $p < 0{,}01$). Es wurden keine signifikanten Unterschiede der rR_2^*-Werte zwischen anderen Lebersegmenten festgestellt.

within each group only occurred in group B, and only in three segments S2, S6 and S7. Note that, as above, relative R_2^* values were closest to 1 in segment 8 for both groups.

The number of patients in different disease groups and their diseases are given in ▶ **Table 3**.

Considering the different reasons for iron overload, there were seven patients in group 1, cf. ▶ **Table 3**. This group showed the lowest mean relative R_2^* (rR_2^*) in segment 1 with 0.92. This means that for this group of patients in segment 1 the R_2^* value was on average 8 % lower than in the other segments. Eleven patients had transfusion-dependent anemia without inadequately increased iron resorption (Group 2, see ▶ **Table 3**). This group contained the participant with the highest rR_2^* of segment 1 (1.13) in our collective. The mean value of rR_2^* in segment 1 was 0.93, the same value as observed in group 3 (n = 26 participants, mostly thalassemia).

Significant differences between patient groups, however, with small effect sizes, were found in segments 3 to 5 and 7. Details are given in ▶ **Table 4**.

▶ **Table 2** Segmental R_2^* values in groups with different mean hepatic R_2^*.

▶ **Tab. 2** Segmentweise R_2^*-Werte der Gruppen mit verschiedenen mittleren R_2^*-Werten der gesamten Leber.

	Whole liver	S1	S2	S3	S4a	S4b	S5	S6	S7	S8
Group A										
Mean R_2^* [s^{-1}]	84.1	79.2	84.4	86.0	83.4	84.9	82.6	82.4	86.0	83.5
StdDev R_2^*	31.5	30.1	32.3	33.4	32.3	34.1	35.6	33.2	30.5	30.4
Mean relative R_2^* (rR_2^*)	–	0.944	1.008	1.025	0.991	1.007	0.971	0.975	1.035	0.993
StdDev relative R_2^*	–	0.072	0.058	0.072	0.045	0.090	0.056	0.075	0.098	0.053
Group B										
Mean R_2^* [s^{-1}]	236.6	216.5	236.1	234.1	236.9	230.4	235.7	240.3	244.6	238.5
StdDev R_2^*	109.8	102.0	103.5	106.5	116.1	102.1	107.3	115.1	115.2	116.1
Significance for R_2^* differences with respect to segment 1 (p)	–	–	0.017*	0.44	0.30	1.00	0.12	0.06	0.005**	0.28
Mean relative R_2^* (rR_2^*)	–	0.909	1.000	0.986	0.993	0.973	1.006	1.016	1.035	1.006
StdDev relative R_2^*	–	0.094	0.086	0.088	0.053	0.074	0.053	0.063	0.070	0.045
Significance for rR_2^* differences with respect to segment 1 (p)	–	–	0.032*	0.302	0.125	1.00	0.055	0.004*	0.0004**	0.072

Mean R_2^* and mean relative R_2^* values for all segments in groups split by mean hepatic R_2^* values. Patients in group A had a mean $R_2^* < 140\ s^{-1}$, patients in group B $R_2^* > 140\ s^{-1}$. For the whole liver, the volumetric R_2^* values are given. The R_2^* values determined by ROIs were 94.7 ± 40.4 s^{-1} (mean ± SD) for group A and 252.9 ± 107.3 s^{-1} (mean ± SD) for group B. There were no significant differences in relative segmental R_2^* values between group A and B. However, significant differences with respect to segment 1 occurred only in group B (marked with * for significant differences, ** for highly significant differences), whereas in group A there were no significant differences between segments at all.
Mittlere R_2^*- und mittlere relative R_2^*-Werte für alle Segmente in den Gruppen, aufgeteilt nach mittleren hepatischen R_2^*-Werten. Die Patienten der Gruppe A hatten einen mittleren R_2^*-Wert < 140 s^{-1}, die Patienten der Gruppe B einen R_2^*-Wert > 140 s^{-1}. Für die gesamte Leber sind die volumetrischen R_2^*-Werte angegeben. Die durch ROIs ermittelten R_2^*-Werte betrugen 94,7 ± 40,4 s^{-1} (Mittelwert ± SD) für Gruppe A und 252,9 ± 107,3 s^{-1} (Mittelwert ± SD) für Gruppe B. Es gab keine signifikanten Unterschiede bei den relativen segmentalen R_2^*-Werten zwischen Gruppe A und B. Signifikante Unterschiede zu Segment 1 traten jedoch nur in Gruppe B auf (gekennzeichnet mit * für signifikante Unterschiede, ** für hochsignifikante Unterschiede), während es in Gruppe A keine signifikanten Unterschiede zwischen den Segmenten gab.

▶ **Table 3** Groups of study participants split by disease.

▶ **Tab. 3** Gruppen der Studienteilnehmer unterteilt nach Krankheitsbildern.

Disease	Male	Female	Sum
Group 1			
Primary Hemochromatosis	4	0	4
Pyruvate Kinase Deficiency	1	0	1
Congenital Dyserythropoietic Anemia	1	0	1
Hemolytic Anemia due to Hb Youngstown	1	0	1
Sum group 1	**7**	**0**	**7**
Group 2			
Diamond Blackfan Anemia	3	2	5
Sickle Cell Disease	0	1	1
Congenital Hemolytic Anemia	0	1	1
Severe Aplastic Anemia	0	1	1
Leukemia after Bone Marrow Transplant	1	1	2
Osteopetrosis	1	0	1
Sum group 2	**5**	**6**	**11**
Group 3			
Thalassemia	11	13	24
MDS after Bone Marrow Transplant	1	1	2
Sum group 3	**12**	**14**	**26**
Overall Sum	**24**	**20**	**44**

Disease patterns and number of participants in different groups, split by the reason for iron overload. Group 1: diseases with increased gastrointestinal iron resorption, but not receiving blood transfusions; group 2: transfusion-dependent anemias with only marginally increased iron resorption; and group 3: diseases requiring transfusion, but also cause increased iron resorption.
Krankheitsbilder und Anzahl der Teilnehmer in verschiedenen Gruppen, aufgeteilt nach dem Grund der Eisenüberladung. Gruppe 1: Erkrankungen mit erhöhter gastrointestinaler Eisenresorption, die jedoch keine Bluttransfusionen erfordern; Gruppe 2: transfusionsabhängige Anämien mit nur geringfügig erhöhter Eisenresorption; und Gruppe 3: Erkrankungen, die eine Transfusion erfordern, aber ebenfalls eine erhöhte Eisenresorption zur Folge haben.

4. Discussion

Liver iron content determination by MRI is widely used today [2, 5, 11–19]. The volumetric acquisition of the liver in a single breath hold and the inline generation of R_2^* maps represent a decisive progress. We used contiguous imaging of the whole liver to analyze segmental R_2^* distribution.

Volumetric evaluation offers an innovative view on the mechanism of hepatic iron accumulation by segmental analysis. It worked well despite limited specific software features for MRI data analysis. Iron overload was studied segment by segment previously, but based on MRI data acquired only in a few slices, with one ROI placed in each segment [20]. The lower relative R_2^* value of segment 1, also called the caudate lobe, compared to the total liver found here is most likely caused by its special vascular supply. R_2^* differences in the other segments may also be caused by different blood flow in various portal vein segments, originating from vessel curvature and diameter, causing some segmental R_2^* differences to be significant, while others are not. Also, outliers, which have a high influence due to small patient numbers, may influence the significance of differences.

The caudate lobe represents a physiologically distinct liver segment that has its own arterial and venous vessel system unlike the rest of the liver parenchyma. Physiologists, therefore, often consider it to be an independent lobe, which is supplied arterially via both the right and left hepatic artery. The venous drainage of the caudate lobe occurs via separate veins (Spieghel veins) directly into the vena cava caudal to the venous star [21]. For this reason, the increased gastrointestinal iron absorption in the majority of diseases in our patient population could have less impact on this segment which may explain the lower R_2^* in the caudate lobe observed in all disease patterns, as well as the smaller differences between S1 and other segments in the group with a lower average R_2^*. It may be of interest that a special vessel situation has previously served as explanation for the aberrant fat content of S4 [22].

To account for the variety of average hepatic R_2^* values, we introduced the relative segmental values. Surprisingly, significant segmental R_2^* differences with respect to the caudate lobe were also found for actual R_2^* values. On the other hand, deviations of segmental R_2^* values from average whole-liver R_2^* values were lowest in segment 8.

Hernando et al. made sure to cover all segments in their recent ROI-based R_2^* analysis of volumetric data but did not address segmental differences [23].

Ghugre et al. found inhomogeneous hepatic iron deposition on different microscopic length scales [24]. Our results indicate non-uniform R_2^* distribution even on a larger scale, pointing to segmental differences in iron concentration. However, we were not able to judge whether there are compartments different from liver segments, but rather restricted our analysis to anatomical liver segments. Probably, a more sophisticated analysis approach like independent component analysis might reveal other functional hepatic subunits than anatomic segments.

R_2^* differences between participant groups were significant in segments 3 to 5 and 7, but not in segment 1. Therefore, the special vascular supply and drainage of S1 did not play a role when comparing disease effects. The group with predominant resorption showed higher rR_2^* than the other groups in S3 to S4b. In S5 and S7, the opposite was observed, while not all differences were significant, c.f. ▶ **Table 3**. These deviations related to underlying diseases possibly point to previously unknown functional disparity of hepatic segments.

It has to be stated that R_2^* differences do not necessarily mean deviations in iron content since GRE sequences are more sensitive to aggregated than to dispersed iron [25]. Also, iron relaxivity was shown to depend on its oxygenation state, namely ferric vs. ferrous ions [26]. However, R_2^* deviations point to metabolic effects differing between segments and disease patterns whether they

▶ **Table 4** Relative and actual R_2^* values for disease groups in selected liver segments.

▶ **Tab. 4** Relative und tatsächlich gemessene R_2^*-Werte der Krankheits-Gruppen in einzelnen Leber-Segmenten.

	Whole liver	Segment 3	Segment 4a	Segment 4b	Segment 5	Segment 7
Relative R_2^* (mean ± SD)						
Group 1	–	1.049 ± 0.055	1.056 ± 0.044	1.023 ± 0.068	0.970 ± 0.028	0.983 ± 0.052
Group 2	–	0.959 ± 0.11	0.982 ± 0.054	0.945 ± 0.091	1.006 ± 0.037	1.032 ± 0.0849
Group 3	–	1.015 ± 0.065	0.978 ± 0.033	1.002 ± 0.079	0.985 ± 0.067	1.050 ± 0.089
Significance for rR_2^* differences (p)						
Group 1 vs. 2	–	0.033 *	0.0098 **	0.042 *	0.026 *	0.113
Group 1 vs. 3	–	0.252	0.002 **	0.66	0.113	0.035 *
Actual R_2^* (mean ± SD)						
Group 1	168.6 ± 113	175.7 ± 114	178.2 ± 122	168.1 ± 103	162.8 ± 109	168.7 ± 121
Group 2	208.5 ± 149	199.9 ± 146	207.3 ± 156	196.3 ± 142	210.2 ± 149	213.3 ± 150
Group 3	143.4 ± 90	144.7 ± 89	141.2 ± 91	144.1 ± 89	142.5 ± 90	149.7 ± 97

Relative and actual R_2^* values in participant groups divided by disease for selected liver segments and significance of relative R2* values for differences between groups. Significant differences are marked by an asterisk. No significant differences were found between groups 2 and 3, and there were no significant differences between segments not mentioned here. There were no significant differences for actual R_2^* values, neither for the whole liver nor for segments.
Relative und tatsächliche R_2^*-Werte für ausgewählte Lebersegmente in den Patientengruppen unterteilt nach Krankheit sowie Signifikanz der Unterschiede der relativen R_2^*-Werte zwischen den Gruppen. Signifikante Unterschiede sind durch ein Sternchen gekennzeichnet. Zwischen den Gruppen 2 und 3 wurden keine signifikanten Unterschiede festgestellt, und auch zwischen den hier nicht aufgeführten Segmenten gab es keine signifikanten Unterschiede. Ebenfalls wurden bei den tatsächlichen R_2^*-Werten keine signifikanten Unterschiede gefunden, weder für die gesamte Leber noch für einzelne Segmente.

are caused by different iron concentrations or a different form or oxygenation state of the iron.

Liver segmentation, which is mandatory for whole-liver volumetric analysis, required time-consuming user interaction in our study. Supported by artificial intelligence, fully automatic segmentation already works reliably enough to enable quick whole-liver volumetric R_2^* analysis [27, 28]. Segmental analysis, however, might still be a challenge at the moment, whereas automated volumetric R_2^* determination has already been introduced.

The exclusion of datasets with insufficient image quality (Likert scores 3 and 4) does not mean that they were unsuitable for volumetric analysis. In order to evaluate feasibility, we wanted to minimize any factors probably affecting preliminary results. Since R_2^* maps were less influenced by sequence limitations than PDFF maps, R_2^* values could have been obtained in all patients with the volumetric approach, but probably while impairing consistency with respect to the ROI-based results.

The sequence used also provided MR-PDFF maps. A detailed presentation of results is beyond the scope of this paper. However, we would like to state that there are PDFF differences between segments which are not congruent to R_2^* differences (manuscript in preparation for submission).

4.1 Limitations

The Liver Health software tool is intended for the evaluation of liver computed tomography data. For MRI liver investigations, a contrast-enhanced T_1-weighted sequence in the hepatobiliary phase is recommended. Since contrast agent is not indicated for liver iron quantification, segmentation was performed on the native data.

Due to its small volume and the difficult definition of the lig. venosum, the segmentation of S1 was most critical. An intra-observer analysis (data not shown) yielded an r value of 0.75 for S1 (and S4b), whereas all other segments were more reliably segmented with $r > 0.8$ for their volume. Regarding segmental R_2^*, however, the r values were > 0.9 for all segments.

To determine the mean parenchymal R_2^*, T_2^* values outside manually defined thresholds were systematically excluded in our approach. A maximum T_2^* value of 50 ms was helpful for the elimination of large vessels, but small vessels could not be handled with this approach because of partial volume effects. Therefore, our results might be influenced by vessel density differing between hepatic segments. An adaptive threshold might be helpful in the future to improve the validity of results.

The inline fitting of the volumetric sequence that was used was a prototype version. In the meantime, the fitting procedure has been optimized to minimize errors like fat-water swaps [29]. First experiences with a new scanner (Magnetom SOLA, Siemens Healthcare GmbH) let us expect that fewer patients will be found to be unsuitable for analysis in the future.

R_2^* analysis was performed in this study solely on patients suspected of having liver iron overload, but not on healthy subjects. It would be of interest to study R_2^* distribution also in healthy subjects and diseases different from conditions causing iron overload. Too few patients in our cohort had normal liver iron content, but

we were able to demonstrate that R_2^* distribution was similar in patients with an LIC below the therapy threshold compared to patients for whom therapy was required. The lack of significance for differences of rR_2^* values observed in S2–8 to S1 for subgroups A and B is probably caused by the small number of participants in these groups. Accordingly, we observed significant rR_2^* differences between segments only in the largest disease subgroup 3 containing 26 participants. Larger studies in healthy subjects might clarify whether relative R_2^* deviations have physiologic reasons or are caused by hematologic diseases.

Dividing patients according to deviating reasons for iron overload led to small subgroups except group 3. Probably due to the small number of patients, segmental relative R_2^* differences were not significant within these subgroups, while a consistent tendency was observed since S1 showed the lowest rR_2^* in all subgroups, whereas the largest rR_2^* value was observed in S7 for all subgroups except group 1 (increased iron absorption).

5. Conclusion

Despite all limitations, the suitability of the tested software for semi-automatic liver segmentation and division into segments based on volumetric MRI data was demonstrated. R_2^* values determined for the whole liver have the advantage of higher reliability and better statistic power due to the larger number of voxels compared to data from individual ROIs drawn on a single slice. Moreover, the volumetric GRE sequence has significant potential beyond single-slice acquisition, e. g. less susceptibility to magnetic field inhomogeneities. Probable benefits of segmental R_2^* determination for the clinical routine should be evaluated with larger patient numbers.

CLINICAL RELEVANCE

- In a volumetric analysis covering the whole liver, we were able to demonstrate that hepatic R_2^* values deviate between segments.
- Segment 7 shows the highest R_2^* except for disease group 1 (increased iron resorption) and should be avoided for LIC determination.
- To minimize sampling errors, segment 8 should be used for noninvasive hepatic iron quantification, since segment 8 shows the least deviations with respect to average whole-liver R_2^*.

Funding

Siemens Healthineers, Master Research Agreement

Conflict of Interest

The Department of Diagnostic and Interventional Radiology has a master research agreement with Siemens Healthcare GmbH. This includes a research grant which gave us access to prototype (works-in-progress) sequences used in this study.Stephan Kannengießer is employee of Siemens Healthcare GmbH.

Acknowledgement

We gratefully acknowledge Yael Glickman, Pedro S. Rodrigues and Hans Peeters from Philips Laboratories for productive discussions.

References

[1] Kang BK, Kim M, Song SY et al. Feasibility of modified Dixon MRI techniques for hepatic fat quantification in hepatic disorders: validation with MRS and histology. Br J Radiol 2018; 91: 20170378

[2] Wood JC, Enriquez C, Ghugre N et al. MRI R_2 and R_2^* mapping accurately estimates hepatic iron concentration in transfusion-dependent thalassemia and sickle cell disease patients. Blood 2005; 106: 1460–1465

[3] Hankins JS, McCarville MB, Loeffler RB et al. R_2^* magnetic resonance imaging of the liver in patients with iron overload. Blood 2009; 113: 4853–4855

[4] Breuer FA, Blaimer M, Mueller MF et al. Controlled aliasing in volumetric parallel imaging (2D CAIPIRINHA). Magn Reson Med 2006; 55: 549–556

[5] Wunderlich AP, Schmidt SA, Mauro V et al. Liver Iron Content Determination Using a Volumetric Breath-Hold Gradient-Echo Sequence With In-Line R(2) * Calculation. J Magn Reson Imaging 2020; 52: 1550–1556

[6] Mory B, Somphone O, Prevost R et al. Real-time 3D image segmentation by user-constrained template deformation. Med Image Comput Comput Assist Interv 2012; 15: 561–568

[7] Sahu S, Schernthaner R, Ardon R et al. Imaging Biomarkers of Tumor Response in Neuroendocrine Liver Metastases Treated with Transarterial Chemoembolization: Can Enhancing Tumor Burden of the Whole Liver Help Predict Patient Survival? Radiology 2017; 283: 883–894

[8] Zhong X, Nickel MD, Kannengiesser SA et al. Liver fat quantification using a multi-step adaptive fitting approach with multi-echo GRE imaging. Magn Reson Med 2014; 72: 1353–1365

[9] Bismuth H. Surgical anatomy and anatomical surgery of the liver. World J Surg 1982; 6: 3–9

[10] Cario H, Grosse R, Janssen G et al. Guidelines for diagnosis and treatment of secondary iron overload in patients with congenital anemia. Klin Padiatr 2010; 222: 399–406

[11] Alustiza JM, Artetxe J, Castiella A et al. MR quantification of hepatic iron concentration. Radiology 2004; 230: 479–484

[12] Andersen PB, Birgegard G, Nyman R et al. Magnetic resonance imaging in idiopathic hemochromatosis. Eur J Haematol 1991; 47: 174–178

[13] Christoforidis A, Perifanis V, Spanos G et al. MRI assessment of liver iron content in thalassamic patients with three different protocols: comparisons and correlations. Eur J Haematol 2009; 82: 388–392

[14] Gandon Y, Olivie D, Guyader D et al. Non-invasive assessment of hepatic iron stores by MRI. Lancet 2004; 363: 357–362

[15] Garbowski MW, Carpenter JP, Smith G et al. Biopsy-based calibration of T_2^* magnetic resonance for estimation of liver iron concentration and comparison with R_2 Ferriscan. J Cardiovasc Magn Reson 2014; 16: 40

[16] Henninger B, Zoller H, Rauch S et al. R_2^* relaxometry for the quantification of hepatic iron overload: biopsy-based calibration and comparison with the literature. Fortschr Röntgenstr 2015; 187: 472–479

[17] St Pierre TG, Clark PR, Chua-anusorn W et al. Noninvasive measurement and imaging of liver iron concentrations using proton magnetic resonance. Blood 2005; 105: 855–861

[18] St Pierre TG, El-Beshlawy A, Elalfy M et al. Multicenter validation of spin-density projection-assisted R_2-MRI for the noninvasive measurement of liver iron concentration. Magn Reson Med 2014; 71: 2215–2223

[19] Wood JC, Pressel S, Rogers ZR et al. Liver iron concentration measurements by MRI in chronically transfused children with sickle cell anemia: baseline results from the TWiTCH trial. Am J Hematol 2015; 90: 806–810

[20] Meloni A, Luciani A, Positano V et al. Single region of interest versus multislice T_2^* MRI approach for the quantification of hepatic iron overload. J Magn Reson Imaging 2011; 33: 348–355

[21] Benkö T, Sgourakis G, Molmenti EP et al. Portal Supply and Venous Drainage of the Caudate Lobe in the Healthy Human Liver: Virtual Three-Dimensional Computed Tomography Volume Study. World J Surg 2017; 41: 817–824

[22] Matsui O, Kadoya M, Takahashi S et al. Focal sparing of segment IV in fatty livers shown by sonography and CT: correlation with aberrant gastric venous drainage. Am J Roentgenol 1995; 164: 1137–1140

[23] Hernando D, Cook RJ, Qazi N et al. Complex confounder-corrected R_2^* mapping for liver iron quantification with MRI. Eur Radiol 2021; 31: 264–275

[24] Ghugre NR, Coates TD, Nelson MD et al. Mechanisms of tissue-iron relaxivity: nuclear magnetic resonance studies of human liver biopsy specimens. Magn Reson Med 2005; 54: 1185–1193

[25] Jensen JH, Tang H, Tosti CL et al. Separate MRI quantification of dispersed (ferritin-like) and aggregated (hemosiderin-like) storage iron. Magn Reson Med 2010; 63: 1201–1209

[26] Dietrich O, Levin J, Ahmadi SA et al. MR imaging differentiation of Fe(2+) and Fe(3+) based on relaxation and magnetic susceptibility properties. Neuroradiology 2017; 59: 403–409

[27] Xu Z, Gabin G, Grimm R et al. A Deep Learning Approach for Robust Segmentation of Livers with High Iron Content from MR Images of Pediatric Patients. 2021. Proc ISMRM:1871

[28] Jimenez-Pastor A, Alberich-Bayarri A, Lopez-Gonzalez R et al. Precise whole liver automatic segmentation and quantification of PDFF and R_2^* on MR images. Eur Radiol 2021; 31: 7876–7887

[29] Henninger B, Plaikner M, Zoller H et al. Performance of different Dixon-based methods for MR liver iron assessment in comparison to a biopsy-validated R_2^* relaxometry method. Eur Radiol 2021; 31: 2252–2262